Mechanics of Advanced Composite Structures 5 (2018) 25–39

Mechanics of Advanced Composite Structures

journal homepage: http://MACS.journals.semnan.ac.ir

Semnan University

Sensitivity Analysis of Fiber-Reinforced Lamina Micro-Electro-Mechanical Switches with Nonlinear Vibration Using a Higher Order Hamiltonian Approach

A. Kabiri [a], S. Sadeghzadeh [b*]

[a] *School of Railway Engineering, Iran University of Science and Technology (IUST), 16846-13114, Tehran, Iran*

[b] *Assistant Professor, Head of Smart Micro/Nano Electro Mechanical Systems Lab (SMNEMS Lab), School of New Technologies, Iran University of Science and Technology (IUST), 16846-13114, Tehran, Iran*

PAPER INFO

Paper history:
Received 2016-09-28
Revised 2017-08-21
Accepted 2017-09-08

Keywords:
nonlinear vibration,
MEMS switches,
higher order Hamiltonian,
sensitivity analysis

ABSTRACT

In this paper, the nonlinear free vibration of fiber-reinforced lamina micro-switches is investigated, and a sensitivity analysis (SA) is given. The switches are modeled as solid rectangular beams consisting of an isotropic matrix with transversely and longitudinally isotropic reinforcements, incorporating a higher order Hamiltonian approach. An SA of the proposed micro-switch is presented by calculating the numerical derivatives of the presented nonlinear model with respect to the design parameters. The SA of geometric parameters, such as dimensionless length, thickness, initial gap, applied voltage, axial load, and effective modules of the system, was conducted using the Sobol method. It was found that the natural frequency varied when changes were made to the proposed parameters; this finding can be used to optimize future designs.

1. Introduction

Micro-electro-mechanical systems (MEMSs) are used in fields such as aerospace, optical, and biomedical engineering, particularly in applications such as micro-switches, transistors, accelerometers, pressure sensors, micro-mirrors, micro-pumps, micro-grippers, and bio-MEMSs [1-4]. MEMSs are merged devices that connect electrical and mechanical components. Studying the dynamic and static behaviors of atomic force microscope (AFM) cantilevers and controlling the vibration of these cantilevers are examples of challenges that involve both electrical and mechanical components [5-8]. Ghalambaz et al. [9] studied the effects of Van der Waals attraction, Casimir force, small size stretching, fringing field, mid-plane stretching, and axial load on the oscillation frequency of resonators.

The inherent intricacy of the nonlinear vibration of MEMSs makes numerical solutions a better choice than analytical ones. The shooting method [10], the differential quadrature method [11], the homotopy analysis method (HAM) [12], the variational approach (VA) [13], the max–min approach (MMA) [14, 15], and the energy balance method (EBM) [16] are some of the numerical and approximate analytical approaches than can be addressed. Ganji et al. [17] applied the EBM and an amplitude frequency formulation (AFF) to govern the approximate analytical solution for the motion of two mechanical oscillators. They showed that in comparison with a fourth-order Runge-Kutta method, their solution is intuitive and useful for solving strongly nonlinear oscillators. When Ganji and Azimi [18] used both the MMA and an AFF to derive an approximate analytical solution

* *Corresponding author. Tel.: +98-21*-73225812; Fax: +98-21-73021482
E-mail address: sadeghzadeh@iust.ac.ir

DOI: 10.22075/MACS.2018.1635.1078

for the free vibrating motion of nonlinear, conservative, single-degree-of-freedom systems, they concluded that both methods had the same results. Both of these methods are convenient for solving nonlinear equations and can also be utilized for a wide range of time and boundary conditions for nonlinear oscillators.

Yildirim, Saadatnia et al. [19] applied the Hamiltonian approach to obtain the natural frequency of a Duffing oscillator; the obtained results were in complete agreement with the approximate frequencies and the exact solution. Askari [20] utilized a higher order Hamiltonian approach to elicit approximate solutions for the model of buckling in a column and mass-spring system. Khan and Akbarzade [21] used a VA, a Hamiltonian approach, and an AFF to analyze a nonlinear oscillator equation in a double-sided clamped micro-beam-based electromechanical resonator. Moreover, Fu et al. [22] applied the EBM to study a nonlinear oscillation problem in a micro-beam model. They used an equation for the free vibration of a micro-beam, based on the Euler–Bernoulli hypothesis, and they compared the results with a fourth-order Runge-Kutta method.

Bayat et al. [23] investigated He's VA to solve the nonlinear vibration of an electrostatically actuated doubly–clamped micro-beam that was equivalent to the first order of a higher Hamiltonian method [24]. They demonstrated that the VA is a good candidate for the precise periodic solution of nonlinear systems. Final results of mentioned works are listed in Table 1.

The pull-in instability of a cantilever nanoactuator model incorporating the effects of surface, fringing field, and Casimir attraction force was investigated in [26]. Furthermore, an approximate analytical model for calculating the pull-in voltage of a stepped cantilever-type radiofrequency (RF) MEMS switch was developed based on the Euler–Bernoulli beam and a modified couple stress theory, and it was validated by a comparison with the finite element results [27].

Micro-composites are a new class of materials used for the mechanical components of MEMSs. Fiber-reinforced composite materials for structural applications are often made in the form of a thin layer, called lamina. It is known that fibers are stiffer and stronger than the same material in bulk form, whereas matrix materials share their common bulk-form properties. Ashrafi et al. [28] presented a detailed theoretical investigation of the utility of carbon nanotube-reinforced composites for designing actuators with low stiffness and high natural frequencies of vibration. The authors investigated the effects of the nanotube aspect ratio, dispersion, alignment, and volume fraction of the elastic modulus and longitudinal wave velocity, and they calculated the bounds on Young's modulus and wave velocity, capturing the trends of other experimental results reported in the literature. Thostenson and Chou [29] simulated the mechanical and physical properties of nanotube-based composite materials. The focus of this research was to develop a fundamental understanding of the structure/size influence of aligned multiwalled carbon nanotubes on the elastic properties of nanotube-based composites. The experimental characterization results were compared with numerical predictions. Hautamaki et al. [30] conducted an experimental evaluation of MEMS strain sensors embedded in composites, examining the effects of wafer geometry and composite plate stiffness on MEMS strain sensors. In another study, Spearing [31] discussed the effects of length scale and material characterization on MEMS design. He presented the MEMS materials set that is derived from three fabrication routes.

In this study, in order to design actuators made from fiber-reinforced composites, a higher order Hamiltonian method [32] was used to obtain an approximate numerical solution. Contrarily to some recent research, such as [23], we showed that the second order result is extremely close to the EBM and exact solutions. The methodology of using a higher order Hamiltonian approach for solving an ordinary differential equation with high nonlinearity is also presented. Numerical comparisons and results were carried out to confirm the correctness and accuracy of the applied method. The ability of the solution for estimating the effect of various parameters on natural frequency is shown and discussed. Sensitivity analysis (SA) of the proposed MEMS device was studied by considering various parameters in the operation of the micro-beam system.

Table 1. Comparison of natural frequency formulas for micro-beams from recent related works

Fu et al. [22]	$\omega_{\mathrm{EBM}} = \sqrt{\dfrac{4a_4 + 3a_5A^2 + 7a_6A^4/3 + 15a_7A^6/8}{a_1A^4 + 2a_2A^2 + 4a_3}}$
Rafieipour et al. [25]	$\square = \dfrac{\sqrt{2}}{4}\sqrt{\dfrac{64a_4 + 48A^2a_5 + 40A^4a_6 + 35A^6a_7}{5A^4a_1 + 6A^2a_2 + 8a_3}}$
Bayat et al. [23]	$\square_{VA} = \dfrac{\sqrt{2}}{4}\sqrt{\dfrac{64a_4 + 48A^2a_5 + 40A^4a_6 + 35A^6a_7}{3A^4a_1 + 4A^2a_2 + 8a_3}}$

2. Mathematical Model

Figures 1 and 2 depict the fiber-reinforced lamina clamped–clamped micro-beam, with length **l**, width **b**, constant thickness **h**, initial gap $\mathbf{g_0}$, and applied voltage **V**. The micro-beam is doubly clamped and placed between two completely fixed electrodes. The applied voltage results from the electric field, which can be divided into a DC polarization and an AC electric field.

Applying an AC electric field or a periodic mechanical load causes the dynamic deflection and vibration of the micro-beam [33]. For more design options and capabilities, computational studies are essential in addition to experiments. However, there are no exact (analytical) closed-form solutions for all boundary conditions of mechanical systems. As a good alternative, the free vibration of MEMSs can be simulated by applying a Galerkin method (GM) and utilizing classical beam theory.

Regarding the effect of mid-plane deformation, the nonlinear partial differential equation of transverse motion could be expressed as follows [34]:

$$\overline{E}I\frac{\partial^4 w}{\partial x^4}+\rho S\frac{\partial^2 w}{\partial t^2}=\left[\overline{N}+\frac{\overline{E}S}{2l}\int_0^l\left(\frac{\partial w}{\partial x}\right)^2\right]\frac{\partial^2 w}{\partial x^2}+ q(x,t), \quad (1)$$

where $\mathbf{w}(\mathbf{x},\mathbf{t})$ is the transverse deflection, **E** is the Young's modulus, **υ** is the Poisson's ratio, and $\overline{\mathbf{E}}$ is the effective modulus of the micro-beam. The quantity of **E** changes with the different thicknesses of the micro-beam, as follows [25]:

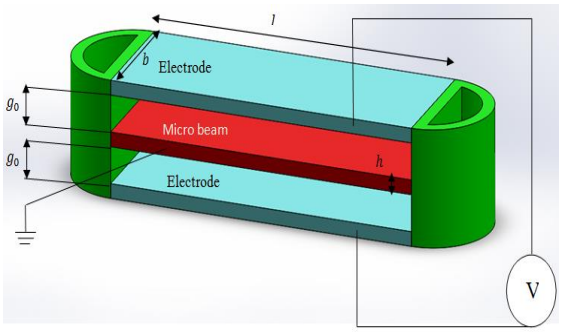

Figure 1. Schematics of doubly-clamped micro-electro-mechanical resonator

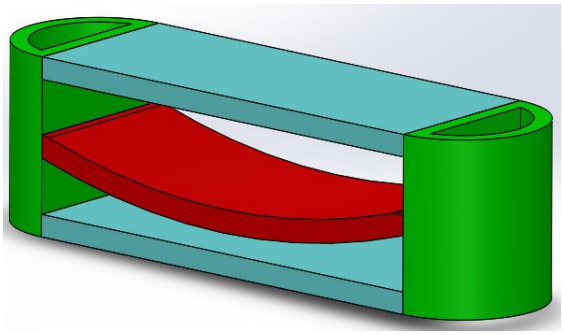

Figure 2. Schematics of deformed micro-electro-mechanical resonator with applied voltage

$$\overline{E}=\begin{cases}\dfrac{E}{1-\upsilon^2} & \text{for wide micro}-\text{beam } (b\geq 5h)\\ E & \text{for narrow micro}-\text{beam } (b<5h)\end{cases} \quad (2)$$

Then, by using a theoretical approach to determine the engineering constants of a continuous fiber-reinforced composite material based on whether the applied loads are parallel or perpendicular to the fiber direction, the effect of fiber-reinforced composite material on the quantity of **E** and **υ** can be expressed in terms of a modulus, Poisson's ratios, and volume fractions of the constituents [35]:

$$E_1=E_fv_f+E_mv_m$$
$$E_2=\frac{E_fE_m}{E_fv_m+E_mv_f} \quad (3)$$
$$\upsilon_{12}=\upsilon_fv_f+\upsilon_mv_m$$

$\mathbf{E_1}$is is the longitudinal modulus, $\mathbf{E_2}$ is the transverse modulus to the fiber direction in the plane of the lamina, $\boldsymbol{\upsilon_{12}}$ is the major Poisson's ratio, $\mathbf{E_f}$ is the modulus of the fiber, and $\mathbf{E_m}$ is the modulus of the matrix; $\boldsymbol{\upsilon_f}$ is the Poisson's ratio of the fiber, $\boldsymbol{\upsilon_m}$ is the Poisson's ratio of the matrix, $\mathbf{v_f}$ is the fiber volume fraction, and $\mathbf{v_m}$ is the matrix volume fraction. Hence, an effective modulus for the micro-beam can be implemented by the following equation for the direction on the laminar plane to be parallel to the fiber:

$$\overline{E}=\begin{cases}\dfrac{E_1}{1-\upsilon_{12}^2} & \text{for a wide micro}-\text{beam } (b\geq 5l\\ E_1 & \text{for a narrow micro}-\text{beam } (b<5l\end{cases} \quad (4)$$

For the direction on the laminar plane to be transverse to the fiber, we would have

$$\overline{E}=\begin{cases}\dfrac{E_2}{1-\upsilon_{12}^2} & \text{for wide micro}-\text{beam } (b\geq 5h)\\ E_2 & \text{for narrow micro}-\text{beam } (b<5h)\end{cases} \quad (5)$$

$\overline{\mathbf{N}}$ Symbolizes the tensile or compressive axial load and is related to the discrepancy of both the thermal expansion coefficient and the crystal lattice period between the substrate and the micro-beam. $\mathbf{q}(\mathbf{x},\mathbf{t})$ is the normalized motivating force that is derived from electrostatic excitation, as follows [36]:

$$q(x,t)=\frac{\varepsilon_v b v^2}{2}\left[\frac{1}{(g_0-w(x,t))^2}-\frac{1}{(g_0+w(x,t))^2}\right], \quad (6)$$

where $\boldsymbol{\varepsilon_v}=\mathbf{8.85\ pF/m}$ is the dielectric constant of the interface. The boundary conditions are as follows:

$$w(0,t)=w(l,t)=0 \quad (7)$$

$$\frac{\partial w}{\partial x}(0,t)=\frac{\partial w}{\partial x}(l,t)=0 \quad (8)$$

The following dimensionless parameters are used to normalize Eq. (1):

$$\xi = \frac{x}{l}, W = \frac{w}{g_0}, \tau = t\sqrt{\frac{\bar{E}I}{\rho bhl^4}}, \quad \alpha = 6\left(\frac{g_0}{h}\right)^2, N = \frac{\bar{N}l^2}{\bar{E}I}, V = \sqrt{\frac{24\varepsilon_v l^4 v^2}{\bar{E}h^3 g_0^3}} \tag{9}$$

Then, dimensionless boundary conditions can be written as follows:

$$W(0,\tau) = W(1,\tau) = 0 \tag{10}$$

$$\frac{\partial W}{\partial x}(0,\tau) = \frac{\partial W}{\partial x}(1,\tau) = 0 \tag{11}$$

Based on the presented formulas, a dimensionless equation of motion can be implemented for MEMS resonators using the following equation:

$$\frac{\partial^4 W}{\partial \xi^4} + \frac{\partial^2 W}{\partial \tau^2} = \left[N + \alpha\int_0^1 \left(\frac{\partial W}{\partial \xi}\right)^2\right]\frac{\partial^2 W}{\partial \xi^2} + \frac{V^2}{4}\left[\frac{1}{(1-W)^2} - \frac{1}{(1+W)^2}\right] \tag{12}$$

By using the assumed modes method, the dimensionless deflection solution of Eq. (12) can be introduced as follows:

$$W(\xi,\tau) = \sum_{i=1}^{n} \phi_i(\xi) u_i(\tau), \tag{13}$$

where $\boldsymbol{\phi_i}(\boldsymbol{\xi})$ is the **i**th Eigen function of a micro-beam that fulfills the appropriate boundary conditions, $\mathbf{u_i}(\boldsymbol{\tau})$ is the **i**th time-dependent deflection coordinate, and **n** is the supposed degree of freedom of the micro-beam.

To solve Eq. (12), we consider a single-degree-of-freedom model ($\mathbf{n = 1}$), and deflection function $\mathbf{W}(\boldsymbol{\xi}, \boldsymbol{\tau})$ is assumed to be as follows:

$$W(\xi,\tau) = \phi(\xi)\, u(\tau) \tag{14}$$

The trial function is

$$\phi(\xi) = 16\,\xi^2(1-\xi)^2. \tag{15}$$

This function satisfies the boundary conditions.

Then, by substituting the presented functions into the dimensionless equation of motion and integrating from 0 to 1, the dimensionless equation of motion changes [22]:

$$\ddot{u}(a_1u^4 + a_2u^2 + a_3) + a_4u + a_5u^3 + a_6u^5 + a_7u^7 = 0 \tag{16}$$

under $u(0) = A, \dot{u}(0) = 0$,

where

$$\begin{aligned}
&a_1 = \int_0^1 \phi^6 d\xi\ ,\ a_2 = 2\int_0^1 \phi^4 d\xi\,,\\
&a_3 = \int_0^1 \phi^2 d\xi\,,\\
&a_4 = \int_0^1 (\phi''''\phi - N\phi''\phi - V^2\phi^2) d\xi\\
&a_5 = \int_0^1 \left(-2\phi''''\phi^3 + 2N\phi''\phi^3 - \alpha\phi''\,\phi\int_0^1(\phi')^2\,d\xi\right) d\xi\\
&a_6 = \int_0^1 \left(\phi''''\phi^5 - N\phi''\phi^5 + 2\alpha\phi''\,\phi^3\int_0^1(\phi')^2\,d\xi\right) d\xi\\
&a_7 = -\int_0^1 \left(\alpha\phi''\,\phi^5\int_0^1(\phi')^2\,d\xi\right) d\xi
\end{aligned} \tag{17}$$

3. Solution Procedure

For the following general oscillator,

$$\ddot{u} + f(u(t)) = 0, \quad u(0) = A, \quad \text{and} \quad \dot{u}(0) = 0, \tag{18}$$

where **u** and **t** are the generalized dimensionless displacement and dimensionless time, respectively, and **A** is the oscillator amplitude. Based on the variational principle, by implementing the semi-inverse [37, 38] and He [13, 39] methods, the variation parameter can be written as

$$J(u) = \int_0^t \left\{-\frac{1}{2}\dot{u}^2 + F(u)\right\} dt, \tag{19}$$

where $\mathbf{T = 2\pi/\omega}$ is the oscillator vibration period and $\frac{\partial \mathbf{F}}{\partial \mathbf{u}} = \mathbf{f(u)}$. Thus, the Hamiltonian approach in the presented problem can be expressed as follows:

$$H = \frac{1}{2}\dot{u}^2 + F(u) = F(A) \tag{20}$$

Then, by defining a new function, we have

$$R(t) = \frac{1}{2}\dot{u}^2 + F(u) - F(A) \tag{21}$$

By choosing any arbitrary point, such as $\boldsymbol{\omega t = \pi/4}$, and setting $\mathbf{R}(\mathbf{t} = \frac{\boldsymbol{\pi}}{\mathbf{4\omega}}) = \mathbf{0}$, an approximate frequency–amplitude relationship can be obtained. This approach is much simpler than other traditional methods and has become widely used [40]. The accuracy of this location method, however, strongly depends upon the chosen location point. To overcome the shortcomings of the EBM, a new approach, based on the Hamiltonian one, has been suggested [32]. Differentiating the Hamiltonian approach leads us to natural frequency of the system:

$$\frac{\partial H}{\partial A} = 0 \tag{22}$$

For greater convenience, a new function, $\widetilde{\mathbf{H}}(\mathbf{u})$, is defined as follows:

$$\widetilde{H}(u) = \int_0^{T/4} \left\{\frac{1}{2}\dot{u}^2 + F(u)\right\} dt = \frac{1}{4}TH \tag{23}$$

Then, for the natural frequencies of the system, the following relation is used:

$$\frac{\partial}{\partial A}\left(\frac{\partial \widetilde{H}}{\partial T}\right) = 0 \ \text{ or } \ \frac{\partial}{\partial A}\left(\frac{\partial \widetilde{H}}{\partial \frac{1}{\omega}}\right) = 0 \tag{24}$$

From Eq. (24), we can obtain the approximate frequency–amplitude relationship of a nonlinear oscillator [32, 41]. For the current special problem, we have the following Hamiltonian equation:

$$\widetilde{H}(u) = \int_0^{T/4} \frac{1}{2}(a_1u^4 + a_2u^2 + a_3)\dot{u}^2 + \left(\frac{1}{2}a_4u^2 + \frac{1}{4}a_5u^4 + \frac{1}{6}a_6u^6 + \frac{1}{8}a_7u^8\right) dt \tag{25}$$

3.1. First-order Hamiltonian approach

After satisfying the initial conditions, utilizing $\mathbf{u} = \mathbf{A}\cos\boldsymbol{\omega}\mathbf{t}$ as the trial function in Eq. (25), we obtain

$$\begin{aligned}\widetilde{H}(u) = \int_0^{\frac{T}{4}} \frac{1}{2}\big(a_1(A\cos\omega t)^4 + \\ a_2(A\cos\omega t)^2 + a_3)(-A\omega\sin\omega t)^2 + \\ \Big(\frac{1}{2}a_4(A\cos\omega t)^2 + \frac{1}{4}a_5(A\cos\omega t)^4 + \\ \frac{1}{6}a_6(A\cos\omega t)^6 + \frac{1}{8}a_7(A\cos\omega t)^8\Big)\,dt\end{aligned} \tag{26}$$

This leads to the following:

$$\begin{aligned}\widetilde{H}(u) = \int_0^{\frac{\pi}{2}} \frac{1}{2}A^2\omega\sin^2 t\,(a_1(A\cos t)^4 + \\ a_2(A\cos t)^2 + a_3) + \frac{1}{\omega}\Big(\frac{1}{2}a_4(A\cos t)^2 + \\ \frac{1}{4}a_5(A\cos t)^4 + \frac{1}{6}a_6(A\cos t)^6 + \\ \frac{1}{8}a_7(A\cos t)^8\Big)\,dt\end{aligned} \tag{27}$$

Then, the frequency–amplitude relationship can be obtained from the following:

$$\begin{aligned}\frac{\partial}{\partial A}\left(\frac{\partial\widetilde{H}}{\partial\frac{1}{\omega}}\right) = 0 \rightarrow A(-0.785a_3 + 0.785a_4\omega^2 + \\ -0.392A^2a_2 + 0.589A^2a_5\omega^2 + \\ -0.294A^4a_1 + 0.490A^4a_6\omega^2 + \\ 0.429A^6a_7\omega^2) = 0\end{aligned} \tag{28}$$

Therefore, after some approximations and simplifications, Eq. (28) can be solved, and the natural frequency can be obtained as follows:

$$\omega \approx \sqrt{\frac{0.785a_4 + 0.589A^2a_5 + 0.490A^4a_6 + 0.429A^6a_7}{0.294A^4a_1 + 0.392A^2a_2 + 0.785a_3}} \tag{29}$$

That is approximately equal to

$$\omega \approx \frac{\sqrt{2}}{4}\sqrt{\frac{64a_4 + 48A^2a_5 + 40A^4a_6 + 35A^6a_7}{3A^4a_1 + 4A^2a_2 + 8a_3}} \tag{30}$$

Both the VA [23] and the analytical approximate solution [25] have the same result for this problem.

3.2. Second-order Hamiltonian approach

To improve the accuracy of this approach, a higher order periodic solution was assumed as the time response function:

$$u = a\cos\omega t + b\cos 3\omega t\,, \tag{31}$$

where the initial condition is

$$A = a + b \tag{32}$$

By Substituting Eq. (32) into Eq. (25), we can obtain

$$\begin{aligned}\widetilde{H}(u) = \int_0^{\frac{\pi}{2}} \frac{1}{2}\omega(a_1(a\cos t + b\cos 3t)^4 + \\ a_2(a\cos t + b\cos 3t)^2 + a_3)(-a\sin t - \\ 3b\sin 3t)^2 + \frac{1}{\omega}\Big(\frac{1}{2}a_4(a\cos t + b\cos 3t)^2 + \\ \frac{1}{4}a_5(a\cos t + b\cos 3t)^4 + \frac{1}{6}a_6(a\cos t + \\ b\cos 3t)^6 + \frac{1}{8}a_7(a\cos t + b\cos 3t)^8\Big)\,dt\end{aligned} \tag{33}$$

Subsequently, the frequency–amplitude relationship can be obtained from the following equation:

$$\begin{aligned}0.343a^5a_1 + 0.392a^3a_2 + 3.239a^4a_1b + \\ 3.926a^2a_2b + 7.068a_3b + 4.417a^3a_1b^2 + \\ 11.191a^2a_1b^3 + 3.534a_2b^3 + 2.650a_1b^5 + \\ 0.196a^3a_5\omega^2 + 0.245a^5a_6\omega^2 + \\ 0.257a^7a_7\omega^2 + 0.785a_4b\omega^2 + \\ 1.178a^2a_5b\omega^2 + 1.472a^4a_6b\omega^2 + \\ 1.803a^6a_7b\omega^2 + 1.472a^3a_6b^2\omega^2 + \\ 3.865a^5a_7b^2\omega^2 + 0.589a_5b^3\omega^2 + \\ 2.945a^2a_6b^3\omega^2 + 7.731a^4a_7b^3\omega^2 + \\ 4.295a^3a_7b^4\omega^2 + 0.490a_6b^5\omega^2 + \\ 5.154a^2a_7b^5\omega^2 + 0.429a_7b^7\omega^2 = 0\end{aligned} \tag{34}$$

To obtain the natural frequency, substituting Eq. (32) into (34) as $\mathbf{b} = \mathbf{A} - \mathbf{a}$, a second-order algebraic equation set becomes solvable, allowing the natural frequency and **a** and **b** values to be obtained for various values of **A** and **V**. Some of the results are listed in Table 2.

3.3. Third-order Hamiltonian approach

A third-order time response can be used for the micro-beam, as follows

$$u = a\cos\omega t + b\cos 3\omega t + c\cos 5\omega t, \tag{35}$$

where the initial condition is

$$A = a + b + c \tag{36}$$

Similar to the second-order Hamiltonian approach, with some mathematical simplification, values of **a**, **b**, **and c** can be obtained for various values of **A** and **V** (see Table 3 for examples).

4. Validation, Results, and Discussion

4.1. Computational efficiency

The nonlinear algebraic equations presented were solved using Wolfram Mathematica software on an Intel(R) Core™ i5-3230M CPU 2.6-GHz processor, including 6 GB of installed memory on a 64-bit operating system. The required time for calculating natural frequencies was 5–10 seconds, 30–40 seconds, and 3.5–4 minutes for first-, second-, and third-order Hamiltonian approaches, respectively. In terms of accuracy and computational efficiency, the second-order solution was the best.

Table 2. a and b parameters for different A and V values ($N = 10, \alpha = 24$)

(A, V)	a	b
(0. 3, 10)	0. 29835	0. 00164
(0. 4, 10)	0. 39554	0. 00445
(0. 5, 10)	0. 49015	0. 00984
(0. 6, 10)	0. 58094	0. 01905
(0. 7, 10)	0. 66653	0. 03346

Table 3. a, b, and c parameters for different A and V values (N = 10, α = 24)

(A, V)	a	b	c
(0. 3, 10)	0. 29830	0. 00165	0. 000046
(0. 4, 10)	0. 39531	0. 00446	0. 000218
(0. 5, 10)	0. 48932	0. 00992	0. 000754
(0. 6, 10)	0. 57849	0. 01937	0. 002135
(0. 7, 10)	0. 66036	0. 03442	0. 005215

4.2. Validation

In comparison with previous works, where higher order approximations were not used, more accurate dynamic responses and natural frequencies were observed. The EBM is the best criterion for such comparisons. Figure 3 depicts a comparison of the dynamic response of a micro-beam under electric excitation (V = 24 Volts), with parameters $\mathbf{N = 10, a = 24, and\ A = 0.4}$ obtained with the first-, second-, and third-order Hamiltonian approaches. These comparisons were repeated (see Fig. 4) after changing the A value to 0.5.

Table 4 compares the frequencies commensurate for different parameters of the system, obtained from the Hamiltonian method and the EBM [22]. Exact values are also reported for some cases. Accuracy increases with an increase in the order of approximations. When the order increases, more accurate results are achieved. Increasing the applied voltage or initial amplitude leads to a greater number of errors. Thus, in the case of larger initial amplitude and applied voltage, higher order approximations would be more useful than lower order ones.

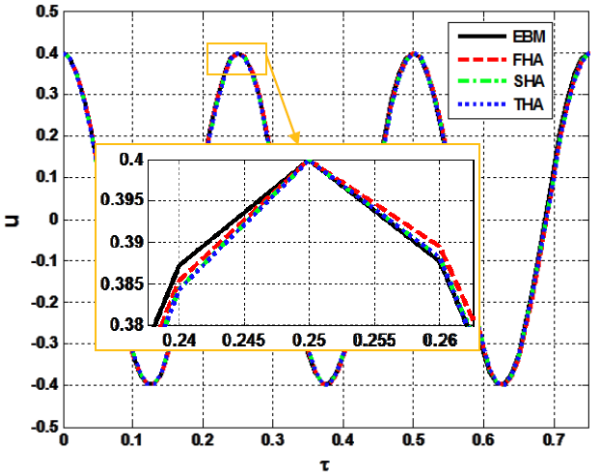

Figure 3. Comparison of dynamic responses obtained using higher order Hamiltonian approaches and an EBM solution ($\mathbf{N = 10, a = 24, V = 10, A = 0.4}$)

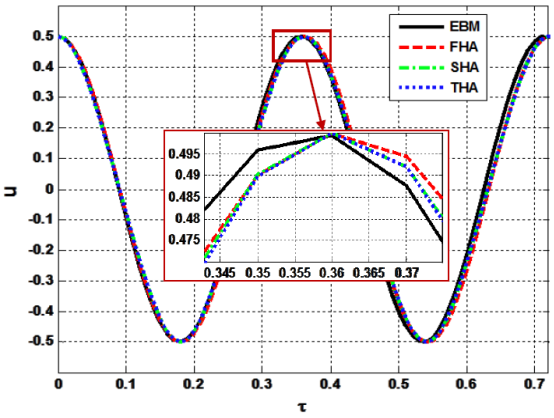

Figure 4. Comparison of dynamic responses obtained using higher order Hamiltonian approaches and an EBM solution ($\mathbf{N = 10, a = 24, V = 20, A = 0.5}$)

4.3. Phase diagram of micro-beam

Simplifying the convolution of a nonlinear system to a pseudo-linear model can provide a useful view on the stability and controllability of a system. For example, let us assume that a nonlinear MEMS micro-beam has a linear-wise model, as below, that includes all nonlinearities in the second part of its dynamics:

$$\dot{x} = Ax + Bu + \Psi_{\text{Nonlinear}}(x, t, u) \tag{37}$$

A nonlinear term ($\boldsymbol{\Psi}_{\mathbf{Nonlinear}}(\mathbf{x}, \mathbf{t}, \mathbf{u})$) may contain a high level of nonlinearity because it includes space, time, and input variables as operands. Figure 5 shows the effect of parameters **A** and **V** on the phase plane of a system for $\mathbf{N = 10, a = 24, and\ V = 5}$, simulated using a second-order Hamiltonian method. As can be seen in Figure 5, by increasing the order of Hamiltonian approach, the amplitude parameters (a, b, c) decrease; thus, the overall amplitude also decreases. When a micro-beam resonates near the zero point as the basal condition, a notable reduction in the velocity of the resonator is observable. This phenomenon disappears immediately after it passes from the basal condition. This means that the dynamics of this nonlinear system also depend on the position of the point that is being measured on the MEMS micro-beam.

Table 4. Comparison of natural frequencies (rad/s) for various parameters of the system ($N = 10, \alpha = 24$)

(A, V)	ω_{VA}	$\omega_{First\ Order}$	$\omega_{Second\ Order}$	$\omega_{Third\ Order}$	ω_{EBM}	ω_{Exact}
(0. 3, 0)	26. 3644	26. 3644	26. 3672	26. 3669	26. 3867	26.8372
(0. 3, 10)	24. 2526	24. 2526	24. 2547	24. 2543	24. 2753	-
(0. 3, 20)	16. 3556	16. 3556	16. 3552	16. 3547	16. 3829	16.6486
(0. 4, 0)	27. 2053	27. 2053	27. 2214	27. 2195	27. 2759	-
(0. 4, 10)	25. 0500	25. 0500	25. 0639	25. 0621	25. 1217	-
(0. 4, 20)	17. 0187	17. 0187	17. 0238	17. 0219	17. 1023	-
(0. 5, 0)	28. 0019	28. 0019	28. 0657	27. 0605	28. 1758	-
(0. 5, 10)	25. 7611	25. 7611	25. 8203	25. 8155	25. 9365	-
(0. 5, 20)	17. 3839	17. 3839	17. 4270	17. 4241	17. 5835	-
(0. 6, 0)	28. 5579	28. 5579	28. 7564	28. 7499	28. 9227	28.5382
(0. 6, 10)	26. 1671	26. 1671	26. 3600	26. 3562	26. 5324	-
(0. 6, 20)	17. 0940	17. 0940	17. 2901	17. 3013	17. 5017	18.5902

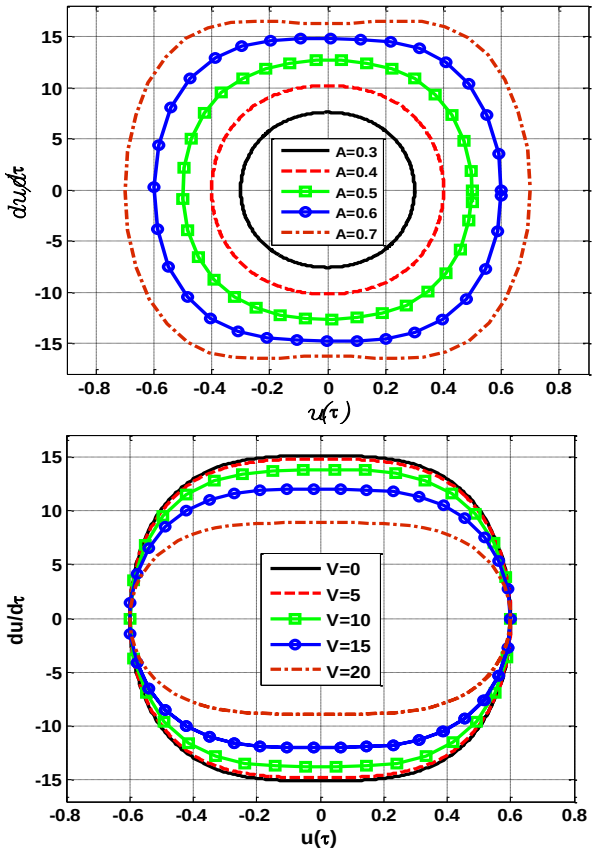

Figure 5. Effect of **A** and **V** parameters on the phase plan of the system for $\mathbf{N = 10}$, $\mathbf{a = 24}$, **and** $\mathbf{V = 5}$ simulated using a second-order Hamiltonian approach

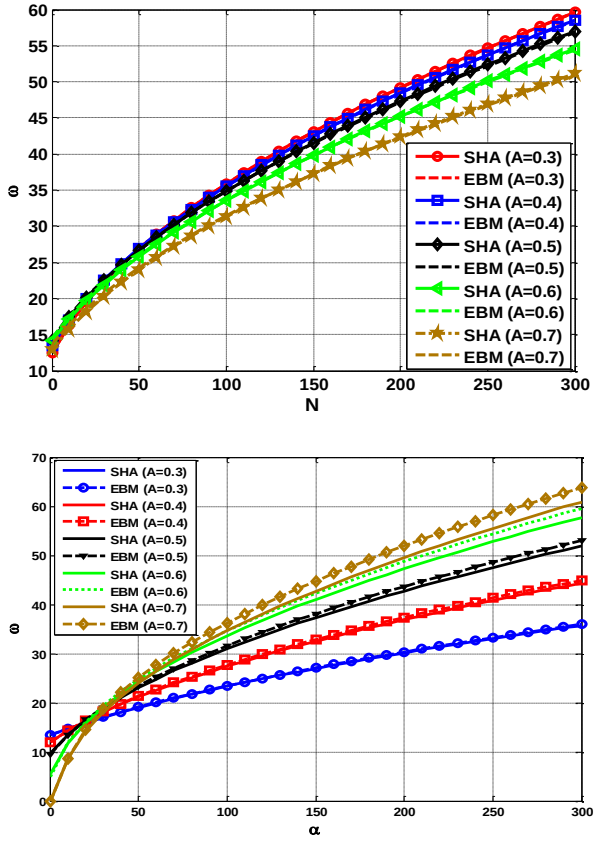

Figure 6. Effect of **N** and **α** parameters on the frequency of an electrostatically actuated micro-beam with $\mathbf{V = 20}$, $\boldsymbol{\alpha} = \mathbf{24}$, $\mathbf{N = 10}$, and various values of **A**

4.4. Free vibration

Figure 6 shows the effect of **N** and **α** parameters on natural frequency. It can be observed that the frequency is proportional to **N**. However, it decreases when initial amplitude (**A**) increases. The second-order Hamiltonian approach has nearly same response as that of the EBM solution, even for higher values of **N** and **A**. Furthermore, it can be observed that the frequency increases with increasing **α**. Results obtained by the second-order Hamiltonian approach are close to the EBM solution, especially for low amplitudes and **α** values.

Figure 7 shows the effect of applied voltage on the natural frequency of an electrostatically actuated micro-beam. It is apparent that the frequency is decreased with an increase in voltage. The results of the second-order Hamiltonian approach are extremely close to the EBM solution, but they have considerable discrepancies in terms of high amplitudes and applied voltages.

The nonlinear behavior of the system leads to an abrupt fall in high applied voltage. The natural frequency decreases dramatically at high voltages. However, natural frequency also increases with an increase in amplitude. This is due to the following effect: when the initial amplitude increases, the equivalent linear system of the electrostatically actuated micro-beam is hardened. It was also observed that for higher amplitudes, the discrepancy is less than that of lower values.

Several simulations and plots can be introduced to facilitate fundamental design requirements before any manufacturing process. Based on the presented examples, the proposed nonlinear model based on a Hamiltonian approach is efficient and sufficiently acceptable to determine the effects of parameters on the natural frequency and the phase plane diagram of an electrostatically actuated micro-beam.

Figures 8 and 9 show the effect of the thickness of an electrostatically actuated micro-beam on the natural frequency at various initial amplitudes when geometrical and structural lamina properties at a fiber-volume fraction of 0.67 are chosen (see Table 5). As demonstrated clearly, natural frequency decreases with an increase in the thickness of a micro-beam.

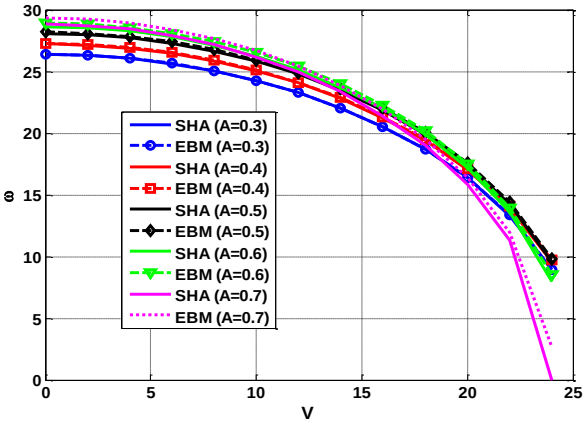

Figure 7. Effect of **V** parameter on the natural frequency of an electrostatically actuated micro-beam with $\mathbf{N} = \mathbf{10}, \boldsymbol{\alpha} = \mathbf{24},$ and various values of **A**

Table 5. Nominal inputs and standard deviations for the micro-switch parameters

Parameter	Value
$l\ (\mu m)$	250
$b\ (\mu m)$	50
$g_0\ (\mu m)$	1
$\bar{N}\ (\mu N)$	1
E_1 (Gpa)	157
E_2 (Gpa)	10.8
υ_{12}	0.3

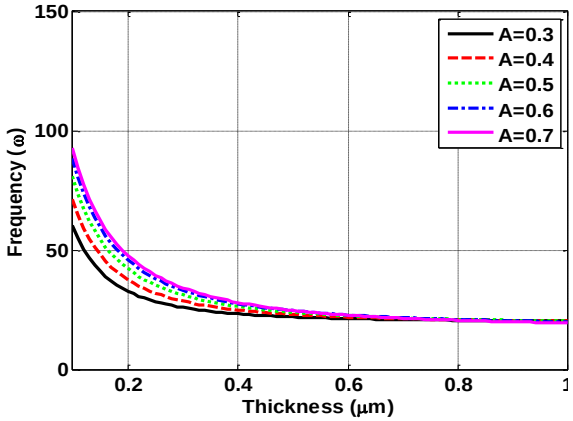

Figure 8. Variation of natural frequency due to the thickness of the micro-beam, thickness (h), where the applied load is parallel to the fiber direction

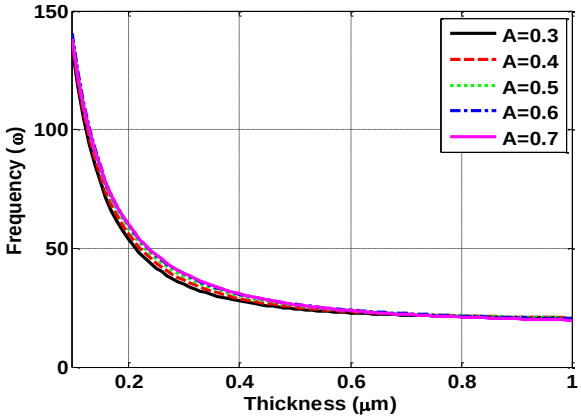

Figure 9. Variation of natural frequency due to the thickness of the micro-beam, (h), where applied load is perpendicular to the fiber direction

5. Sensitivity analysis

When a sensor or actuator is designed based on micro-beams, recognizing the parameters can help the designer to obtain the best resolution and accuracy. This issue can be addressed by conducting SA on electrostatically actuated micro-beams. Thus, SA of the model, with respect to the model parameters, is a key step. SA can classify the values of various significant parameters according to the proposed research preferences [43].

Various parameters contribute to the final responses in any nonlinear system under considera-

tion. Parameters include the length **l**, width **b**, thickness **h**, Young's modulus, and Poisson's ratio of a micro-beam on the one hand and the initial gap $\mathbf{g_0}$, electrostatic load **V**, **α** , **and N** on the other. This model requires the identification of many parameters and inputs at varying levels of sensitivity, and various SA methods can be used to achieve this requirement. The Sobol method is a famous SA approach based on variance that is widely used in various studies and scientific fields, such as hydrogeology, geotechnics, ocean engineering, biomedical engineering, hybrid dynamic simulation, and electromagnetism.

5.1. Simple form of sensitivity

A simple form of determining sensitivity for natural frequency respecting these parameters could be achieved by differentiating the natural frequency with respect to the parameters and plotting the results (e.g., Figure 10). Below, $\mathbf{S_\alpha^\omega}$ represents the sensitivity of **ω** with respect to the variation of parameter **α**:

$$S_\alpha^\omega = \frac{\partial \omega}{\partial \alpha} \tag{38}$$

Using the parameters introduced in Table 5, Figs. 10 to 13 are presented to depict variations in sensitivity with respect to various parameters. Figure 10 shows the sensitivity of an electrostatically actuated micro-beam with respect to parameter **α**. It can be observed that sensitivity decreases with increases in parameter **α**. Since $\boldsymbol{\alpha = 6\left(\frac{g_0}{h}\right)^2}$ in the presented sensitivity plot, this means that if $\mathbf{g_0}$ increases or **h** decreases, the micro-beam reacts less easily to external excitations. Increasing the thickness increases the system rigidity, which makes the micro-beamless sensitive. In contrast, decreasing the gap between the beam and the electrodes of an electrostatically actuated micro-beam results in a lower excitation output.

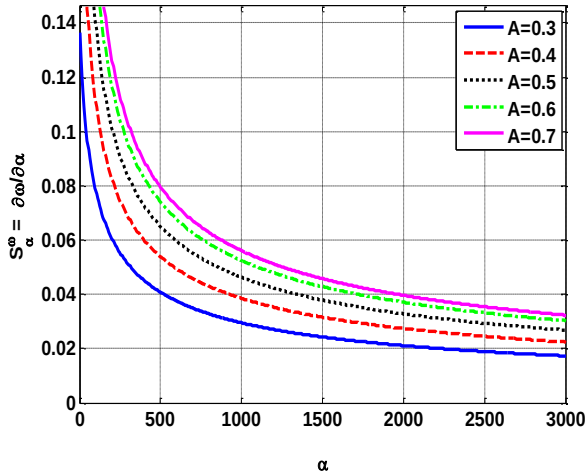

Figure 10. Sensitivity plot of an electrostatically actuated micro-beam with respect to the variation of parameter **α** with $\mathbf{N = 10}$, $\mathbf{V = 20}$, and various amplitudes

Figure 11 depicts micro-beam sensitivity versus the external load. With increased external loads, sensitivity decreases because of the rigidity. The rigidity increases due to system hardening, which is caused by higher external loads.

Figure 12 shows a sensitivity plot of a micro-beam with respect to the applied voltage. By applying more voltage, a less-sensitive sensor and actuator can be achieved. Although more sensitivity is a good option for low applied voltages, supplementary equipment for detecting and exciting the system would be extremely challenging. Therefore, it is not suggested for practical purposes.

In Figure 13, a sensitivity plot of a micro-beam with respect to the modulus of elasticity is shown. The modulus of elasticity can be considered to be about 700 GPa. Greater hardness leads to greater sensitivity, so any approach that increases the stiffness of a micro-beam improves its efficiency. Carbon-fiber reinforced nanostructures improve the electromechanical properties [44].

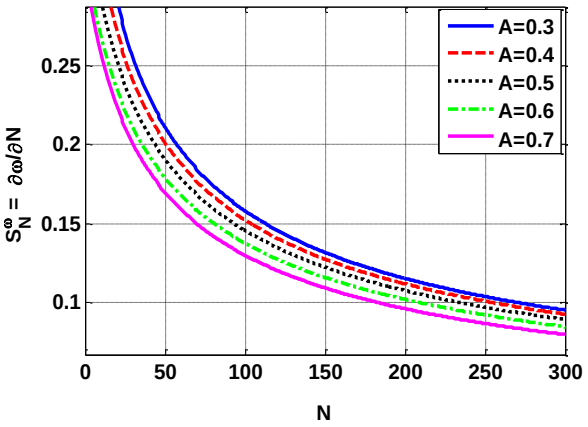

Figure 11. Sensitivity plot of an electrostatically actuated micro-beam with respect to the variation of parameter **N** with $\mathbf{\alpha = 24, V = 20}$, and various amplitudes

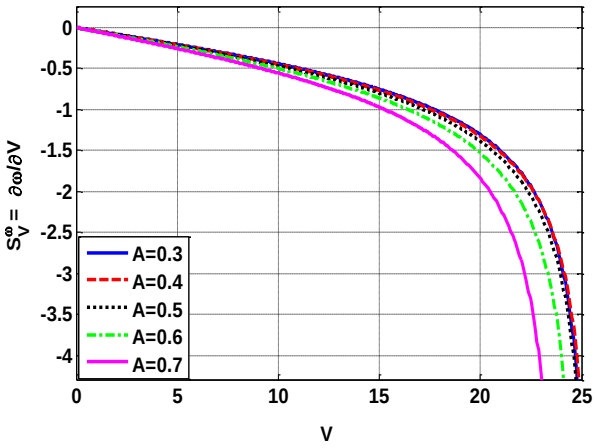

Figure 12. Sensitivity plot of an electrostatically actuated micro-beam with respect to the variation of parameter **V** with $\mathbf{N = 10, \alpha = 24,}$ and various amplitudes

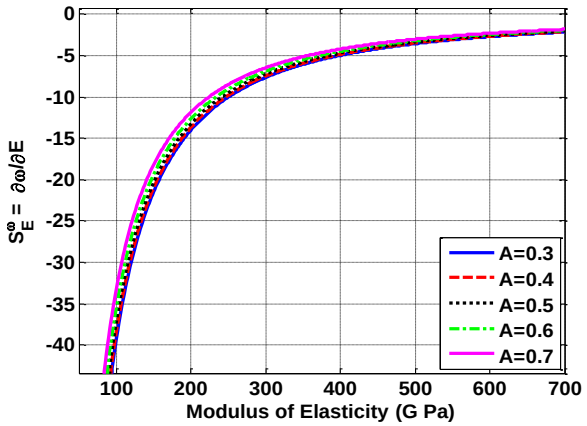

Figure 13. Sensitivity plot of an electrostatically actuated micro-beam with respect to the variation of parameter $\bar{E}$ with various amplitudes

5.2. The Sobol method of global sensitivity

The Sobol method for nonlinear models is used here to achieve an optimal design. This method was used to investigate the effects of a geometrical parameter on the natural frequency when all other parameters are changing at the same time. The inputs are changed, and the effect of each one on the model output is analyzed.

For nonlinear mathematical models with numerous inputs, it is often difficult to anticipate the response of the model output to changes in the inputs. Complicated interactions of physical processes mean that varying one input parameter at a time does not adequately characterize the range of possible model outputs, although a one-at-a-time analysis may be valuable as a preliminary screening exercise. A comprehensive SA must examine the response of the model to changes in all parameters across their range of values; this is known as global SA.

Between different general sensitivity analyses, variance-based methods are gaining the most attention. In these methods, the sensitivity index is computed as the share of each parameter in the overall output variance of the model. The Sobol method [45] is an independent general SA method based on variance analysis.

We consider a computer model $\mathbf{Y}$, and thus, this relation can be written as follows:

$$Y = f(x_1, x_2, \dots, x_n), \tag{39}$$

where n is the number of independent parameters.

The input independent parameter region should be determined as follows to explain the Sobol's method:

$$\Omega^n = \left(X \middle| x_i^{min} < x_i < x_i^{max}; i = 1, \dots, n\right), \tag{40}$$

where $\mathbf{x_i^{min}}$ and $\mathbf{x_i^{max}}$ are the minimum and maximum values for $\mathbf{x_i}$, respectively.

The Sobol sensitivity indices are ratios of partial variances to the total variance. We can subdivide them into partial variances of increasing dimensionality:

$$V(Y) = \sum_i^n V_i + \sum_i^n \sum_{j>i}^n V_{ij} + \cdots + V_{12\dots n}, \tag{41}$$

where for any input $\mathbf{i}$, $\sum_{\mathbf{i}}^{\mathbf{q}} \mathbf{V_i}$ is called its first-order or main effect sensitivity index, $\sum_{\mathbf{i}}^{\mathbf{n}} \sum_{\mathbf{j>i}}^{\mathbf{n}} \mathbf{V_{ij}}$ includes all the partial variances of interaction of two input parameters, and so on.

The representation of function $\mathbf{Y}$ is derived from the sum of the following functions:

$$f(x_1, x_2, \dots, x_n) = f_0 + \sum_{i=1}^n f_i(x_i) + \sum_{1 \le i \le j \le n} f_{ij}(x_i, x_j) + \cdots + f_{1,2,\dots,k}(x_1, x_2, \dots, x_n), \tag{42}$$

where $\mathbf{f_0}$ is constant and is determined as follows:

$$f_0 = \int_{\Omega^n} f(x) fx \tag{43}$$

Sobol showed that the decomposition of Eq. (25) is unique. Also, all terms of the mentioned equation can be evaluated via the following multidimensional integrals:

$$f_i(x_i) = -f_0 + \int_0^1 \dots \int_0^1 f(x) dx_{\sim i} \tag{44}$$

$$f_{ij}(x_i, x_j) = -f_0 - \sum f_i(x_i) + \int_0^1 \dots \int_0^1 f(x) dx_{\sim ij}, \tag{45}$$

where $\mathbf{dx_{\sim i}}$ **and** $\mathbf{dx_{\sim ij}}$ show the integration over all the variables, excluding $\mathbf{x_i}$ and $\mathbf{x_j}$, respectively. Hence, for higher order terms, a continuous formula can be obtained. In the sensitivity indices based on variance, the total variance of $\mathbf{f(x)}$, $\mathbf{V}$ is expressed as

$$V = \int f^2(x)\, dx - (f_0)^2 \tag{46}$$

Partial variances are computed as follows:

$$V_{i_1,\dots,i_n} = \int_{\Omega^n} f_{i_1,\dots,i_n}^2(x_{i_1}, \dots, x_{i_n}) dx - (f_0)^2 \tag{47}$$

According to Eq. (41), the sensitivity measures $\mathbf{S_{1,2,\dots,k}}$ are given by

$$S_{1,2,\dots,n} = \frac{V_{1,2,\dots,n}}{V} \quad , \quad 1 \le i_1 \le \cdots \le i_n \tag{48}$$

The measure of the first order $\mathbf{S_i}$ evaluates the contribution of the variation of $\mathbf{x_i}$ to the total variance of Y. The measure of the second order of $\mathbf{S_{ij}}$ evaluates the contribution of the interaction of $\mathbf{x_i}$ and $\mathbf{x_j}$ on the output, and so on.

By applying Sobol's sensitivity, the effect of the electrostatically actuated micro-beam parameters on the frequency of the system can be obtained. The first

step in SA is to determine the ranges of the model inputs. Defining the probability distribution of inputs requires the use of sample-based methods (e.g., a variance-based method or the Monte Carlo SA method). How the input parameters are chosen and how their ranges are determined basically depends on the objectives of the SA. In this study, we have analyzed four dimensionless parameters ($\bar{\mathbf{E}}$, **N**, **α**, **and V**) to predict the influence of various parameters of an electrostatically actuated micro-beam.

5.2.1 Steps for implementation

Sobol's algorithm can be summarized by the following steps:

1. Select the total number of simulations to be performed.
2. Select the parameters for SA.
3. Determine ranges for test variables.
4. Choose a distribution for each of the parameters. In this case, a uniform distribution is chosen for all four parameters.
5. Calculate the variance of the parameters using Eq. (47).
6. Compute the partial variance or first order effects for each parameter by fixing the values of that parameter and varying the remaining parameters.
7. Calculate the total-order index of the parameters using Eq. (48).
8. Sort the parameters according to their sensitivities.

Figure 14 shows the effects of dimensionless parameters on the natural frequency, including Young's modulus, an axial force toward the beam, applied voltage, and the ratio of the gap between the beam and the electrodes to the thickness of the beam, via the Sobol method. As is observable, by increasing the applied initial amplitude, the effects of different parameters change, and at higher frequencies, the term $\boldsymbol{\alpha}\ (\mathbf{6}\left(\frac{\mathbf{g_0}}{\mathbf{h}}\right)^{\mathbf{2}})$ has the greatest influence on the natural frequency.

In clamped–clamped beams, the abovementioned ratio (beam–electrode gap to beam thickness) exerts the greatest influence on the natural frequency, and the length of the beams has the second-greatest influence on this frequency. The applied voltage and Young's modulus are effective on frequencies at low amplitudes, but these effects can be ignored at high amplitudes. The axial force also has an ignorable influence on the frequency.

6. Conclusion

The sensitivity of a micro-switch containing a doubly clamped micro-beam with length **l**, width **b**, and constant thickness **h** ($\mathbf{b} \geq \mathbf{5h}$); effective modulus $\bar{\mathbf{E}}$; initial gap $\mathbf{g_0}$; and electrostatic applied voltage **V** is studied by using a higher order Hamiltonian approach. A nonlinear partial differential equation of the transverse motion resulting from mid-plane deformation has been expressed, and the normalized motivating force has been calculated based on electrostatic excitation. A dimensionless equation of motion has been derived based on the variational principle. By implementing a semi-inverse method and exploiting He's method, an approximate frequency–amplitude relationship has been obtained. Differentiating the Hamiltonian approach reveals the natural frequency of micro-switches. The overall results of this study are listed below.

6.1. Comparisons

1. The VA and the analytical approximate solution had the same results for this problem.
2. The time required for calculating natural frequencies using the proposed specific computational platform was 5–10 seconds, 30–40 seconds, and 3.5–4 minutes for first-, second-, and third-order Hamiltonian approaches, respectively. The second-order solution was the most efficient computationally and in terms of accuracy.
3. The obtained results have been validated in comparison with the EBM, in which higher order approximations are neglected.
4. By increasing the order of approximation, the accuracy of the proposed method increases.
5. Increasing the applied voltage or initial amplitude leads to more errors. Thus, in the case of a higher initial amplitude and applied voltage, higher order approximations are essential.

6.2. Natural frequency calculations

1. The natural frequency increases as **N** increases. However, it decreases in accordance with an increase of the initial amplitude (**A**). Nevertheless, the second-order Hamiltonian approach produces an extremely close response to that of the EBM solution, even for higher values of **N** and higher amplitude. Natural frequency also decreases with amplitude increasing.
2. The natural frequency increases with increasing values of **α**. Results of the second-order Hamiltonian approach are close to the EBM solution except for high amplitude and **α** values. The natural frequency also decreases as the voltage increases. The results of the second-order Hamiltonian approach are extremely close to the EBM solution aside from considerable discrepancies in high amplitudes and voltages.

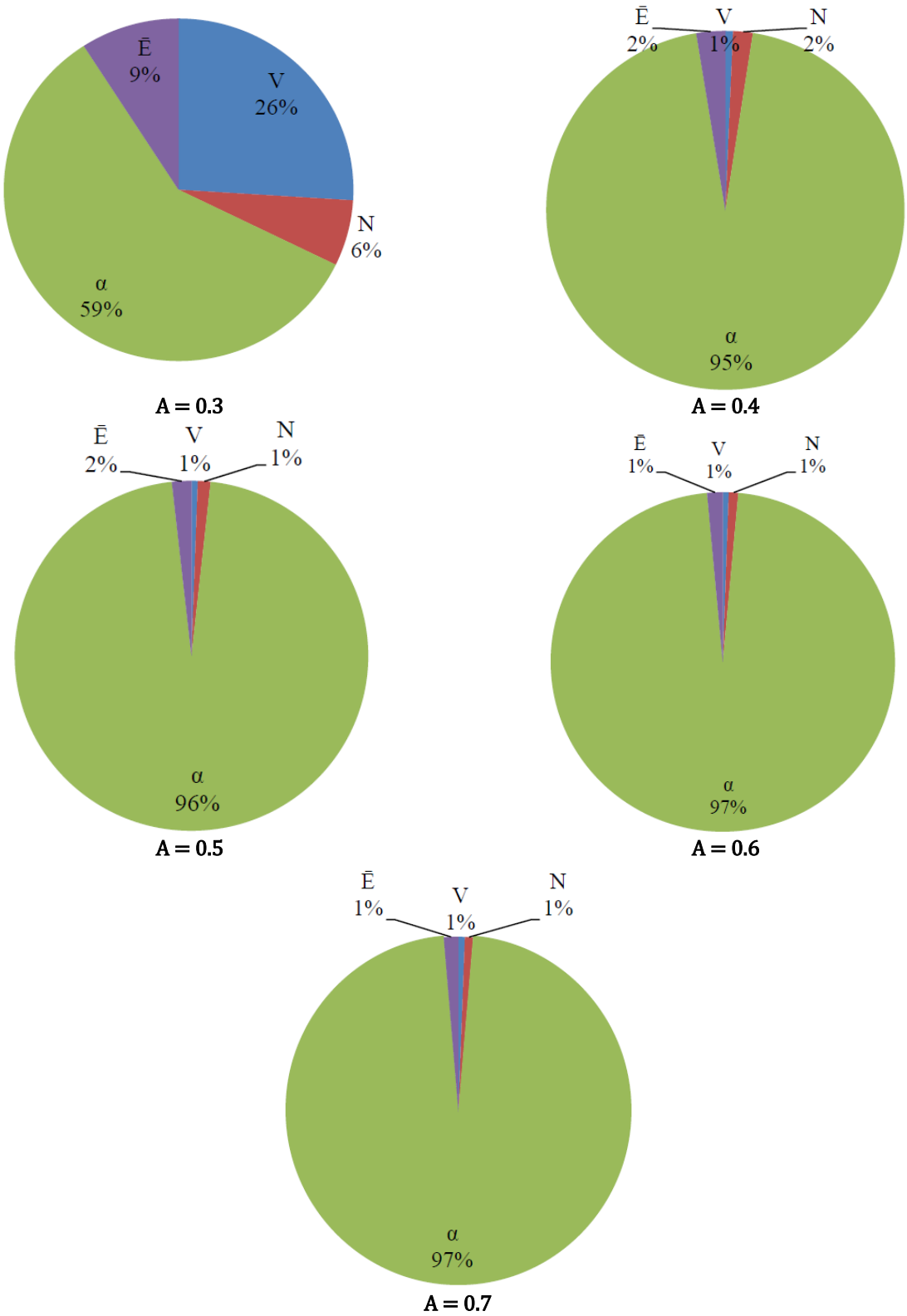

Figure 14. Pie chart diagrams of Sobol's sensitivity analysis (SA) of an electrostatically actuated micro-beam with respect to the variation of $\bar{E}$, **N**, **α**, **and V** parameters with various amplitudes

1. The nonlinear behavior of the system leads to an abrupt fall in high applied voltages. The natural frequency decreases dramatically at high voltages and also decreases at low voltages.
2. The natural frequency increases with an increase in the modulus of elasticity and decreases with increasing thickness of the micro-beam; however, these variations are not significant

6.3. Sensitivity analysis

1. Sensitivity decreases when $\boldsymbol{\alpha}$ increases. As $\boldsymbol{\alpha}$ is equal to $6\left(\frac{g_o}{h}\right)^2$, the presented sensitivity plot (i.e. Fig. 10) means that if $\mathbf{g_o}$ increases or $\mathbf{h}$ decreases, the micro-beam reacts less to external excitations. By increasing the thickness, rigidity also increases, which leads to less sensitivity of the micro-beam. However, decreasing the gap between the beam and the electrodes an of electrostatically actuated micro-beam results in a lower excitation output.
2. With increased external loads, the sensitivity decreases because of increased rigidity; the rigidity increases due to system hardening caused by increased external loads.
3. By applying more voltage, a less-sensitive sensor and actuator can be achieved. Although greater sensitivity seems to be a good option for low levels of applied voltage, providing supplementary equipment for detecting and exciting the system would be extremely challenging; therefore, it is not suggested for practical purposes.
4. By the Sobol method, it was shown that at higher frequencies, the variable $\boldsymbol{\alpha}$ ($6\left(\frac{g_o}{h}\right)^2$) has the greatest influence on the natural frequency. In clamped–clamped beams, the ratio of the gap between the beam and the electrodes to the thickness of the beam has the most influence on the natural frequency, followed by the length of the beams (ranked second most influential). The axial force also has an insignificant effect on frequency.

References

[1] Yogeswaran U, Thiagarajan S, Chen S-M. Recent updates of DNA incorporated in carbon nanotubes and nanoparticles for electrochemical sensors and biosensors. *Sensors* 2008; 8(11): 7191-212.

[2] Allen BL, Kichambare PD, Star A. Carbon nanotube field-effect-transistor-based biosensors. *Adv. Mater.* 2007; 19(11): 1439-51.

[3] Atashbar MZ, Bejcek B, Singamaneni S, Santucci S. (2004). *Carbon nanotube based biosensors.* Paper presented at the Sensors, 2004. Proceedings of IEEE.

[4] Jain A, Goodson KE. Thermal microdevices for biological and biomedical applications. *Journal of Thermal Biology* 2011; 36(4): 209-18.

[5] Korayem M, Sadeghzadeh S, Homayooni A. Semi-analytical motion analysis of nano-steering devices, segmented piezotube scanners. *International Journal of Mechanical Sciences* 2011; 53(7): 536-48.

[6] Korayem M, Homayooni A, Sadeghzadeh S. Semi-analytic actuating and sensing in regular and irregular MEMs, single and assembled micro cantilevers. *Applied Mathematical Modelling* 2013; 37(7): 4717-32.

[7] Korayem M, Sadeghzadeh S, Homayooni A. Coupled dynamics of piezo-tube and microcantilever in scanning probe devices and sensitive samples imaging. *Micro & Nano Letters* 2012; 7(9): 986-90.

[8] Korayem M, Karimi A, Sadeghzadeh S. GDQEM analysis for free vibration of V-shaped atomic force microscope cantilevers. *International Journal of Nanoscience and Nanotechnology* 2014; 10(4): 205-14.

[9] Ghalambaz M, Ghalambaz M, Edalatifar M. Nonlinear oscillation of nanoelectro-mechanical resonators using energy balance method: considering the size effect and the van der Waals force. *Applied Nanoscience* 2016; 6(3): 309-17.

[10] Abdel-Rahman EM, Younis MI, Nayfeh AH. Characterization of the mechanical behavior of an electrically actuated microbeam. *Journal of Micromechanics and Microengineering* 2002; 12(6): 759.

[11] Kuang J-H, Chen C-J. Dynamic characteristics of shaped micro-actuators solved using the differential quadrature method. *Journal of Micromechanics and Microengineering* 2004; 14(4): 647.

[12] Beléndez A, Beléndez T, Márquez A, Neipp C. Application of He's homotopy perturbation method to conservative truly nonlinear oscillators. *Chaos, Solitons & Fractals* 2008; 37(3): 770-80.

[13] He J-H. Variational approach for nonlinear oscillators. *Chaos, Solitons & Fractals* 2007; 34(5): 1430-9.

[14] He J-H. Max-min approach to nonlinear oscillators. *International Journal of Nonlinear Sciences and Numerical Simulation* 2008; 9(2): 207-10.

[15] Zeng D, Lee Y. Analysis of strongly nonlinear oscillator using the max-min approach.

International Journal of Nonlinear Sciences and Numerical Simulation 2009; 10(10): 1361-8.
[16] He J-H. Preliminary report on the energy balance for nonlinear oscillations. *Mechanics Research Communications* 2002; 29(2-3): 107-11.
[17] Ganji DD, Azimi M, Mostofi M. Energy balance method and amplitude frequency formulation based simulation of strongly non-linear oscillators. 2012.
[18] Ganji DD, Azimi M. Application of max min approach and amplitude frequency formulation to nonlinear oscillation systems. *UPB Scientific Bulletin* 2012; 74(3): 131-40.
[19] Yildirim A, Askari H, Yazdi MK, Khan Y. A relationship between three analytical approaches to nonlinear problems. *Applied Mathematics Letters* 2012; 25(11): 1729-33.
[20] Askari H, Nia ZS, Yildirim A, Yazdi MK, Khan Y. Application of higher order Hamiltonian approach to nonlinear vibrating systems. *Journal of Theoretical and Applied Mechanics* 2013; 51(2): 287-96.
[21] Khan Y, Akbarzade M. Dynamic analysis of nonlinear oscillator equation arising in double-sided driven clamped microbeam-based electromechanical resonator. *Zeitschrift für Naturforschung A* 2012; 67(8-9): 435-40.
[22] Fu Y, Zhang J, Wan L. Application of the energy balance method to a nonlinear oscillator arising in the microelectromechanical system (MEMS). *Current applied physics* 2011; 11(3): 482-5.
[23] Bayat M, Bayat M, Pakar I. Nonlinear vibration of an electrostatically actuated microbeam. *Latin American Journal of Solids and Structures* 2014; 11(3): 534-44.
[24] Yildirim A, Saadatnia Z, Askari H, Khan Y, KalamiYazdi M. Higher order approximate periodic solutions for nonlinear oscillators with the Hamiltonian approach. *Applied Mathematics Letters* 2011; 24(12): 2042-51.
[25] Rafieipour H, Lotfavar A, Masroori A. Analytical approximate solution for nonlinear vibration of microelectromechanical system using he's frequency amplitude formulation. *Iranian Journal of Science and Technology. Transactions of Mechanical Engineering* 2013; 37(M2): 83.
[26] Duan J, Li Z, Liu J. Pull-in instability analyses for NEMS actuators with quartic shape approximation. *Applied Mathematics and Mechanics* 2016; 37(3): 303-14.
[27] Zhu J, Liu R. Sensitivity analysis of pull-in voltage for RF MEMS switch based on modified couple stress theory. *Applied Mathematics and Mechanics* 2015; 36(12): 1555-68.
[28] Ashrafi B, Hubert P, Vengallatore S. Carbon nanotube-reinforced composites as structural materials for microactuators in microelectromechanical systems. *Nanotechnology* 2006; 17(19): 4895.
[29] Thostenson ET, Chou T-W. On the elastic properties of carbon nanotube-based composites: modelling and characterization. *J. Phys. D: Appl. Phys.* 2003; 36(5): 573.
[30] Hautamaki C, Zurn S, Mantell SC, Polla DL. Experimental evaluation of MEMS strain sensors embedded in composites. *Journal of microelectromechanical systems* 1999; 8(3): 272-9.
[31] Spearing S. Materials issues in microelectromechanical systems (MEMS). *Acta Mater.* 2000; 48(1): 179-96.
[32] He J-H. Hamiltonian approach to nonlinear oscillators. *Phys. Lett. A* 2010; 374(23): 2312-4.
[33] Younis MI, Nayfeh A. A study of the nonlinear response of a resonant microbeam to an electric actuation. *Nonlinear Dynamics* 2003; 31(1): 91-117.
[34] Rao SS. **Vibration of continuous systems**. John Wiley & Sons; 2007.
[35] Reddy JN. **Mechanics of laminated composite plates and shells: theory and analysis**. CRC press; 2004.
[36] Pelesko JA, Bernstein DH. **Modeling Mems and Nems**. CRC press; 2002.
[37] He J-H. Semi-inverse method of establishing generalized variational principles for fluid mechanics with emphasis on turbomachinery aerodynamics. *International Journal of Turbo and Jet Engines* 1997; 14(1): 23-8.
[38] He J-H. Variational principles for some nonlinear partial differential equations with variable coefficients. *Chaos, Solitons & Fractals* 2004; 19(4): 847-51.
[39] Bayat M, Pakar I. Application of Hes energy balance method for nonlinear vibration of thin circular sector cylinder. *International Journal of Physical Sciences* 2011; 6(23): 5564-70.
[40] Jamshidi N, Ganji D. Application of energy balance method and variational iteration method to an oscillation of a mass attached to a stretched elastic wire. *Current Applied Physics* 2010; 10(2): 484-6.
[41] Shou D-H. Variational approach for nonlinear oscillators with discontinuities. *Computers & Mathematics with Applications* 2009; 58(11-12): 2416-9.
[42] Qian Y, Ren D, Lai S, Chen S. Analytical approximations to nonlinear vibration of an electrostatically actuated microbeam. *Communications in Nonlinear Science and Numerical Simulation* 2012; 17(4): 1947-55.
[43] Saltelli A, Homma T. Sensitivity analysis for model output: performance of black box

techniques on three international benchmark exercises. *Computational statistics & data analysis* 1992; 13(1): 73-94.

[44] Hong W-l, Guo X-m. Deformation of metallic single-walled carbon nanotubes in electric field based on elastic theory. *Applied Mathematics and Mechanics* 2010; 31(3): 271-8.

[45] Sobol' IyM. On sensitivity estimation for nonlinear mathematical models. *Matematicheskoe modelirovanie* 1990; 2(1): 112-8.